Robotica (2014) volume 32, pp. 625–641. © Cambridge University Press 2013
doi:10.1017/S0263574713000854

Dynamic 3D modeling and simulation of nanoparticles manipulation using an AFM nanorobot

M. H. Korayem* and A. K. Hoshiar

Department of Mechanical and Aerospace Engineering, Science and Research Branch, Islamic Azad University, Tehran, Iran

(Accepted August 2, 2013. First published online: October 8, 2013)

SUMMARY

Due to the growing use of Atomic Force Microscope (AFM) nanorobots in the moving and manipulation of cylindrical nanoparticles (carbon nanotubes and nanowires) and the fact that these processes cannot be simultaneously observed, a computer simulation of the involved forces for the purpose of predicting the outcome of the process becomes highly important. So far, no dynamic 3D model that shows changes in these forces in the course of process implementation has been presented. An algorithm is used in this paper to show in 3D, the manner by which the dynamic forces vary in the mentioned process. The presented model can simulate the forces exerted on the probe tip during the manipulation process in three directions. Because of the nonlinearity of the presented dynamic model, the effective parameters have been also studied. To evaluate the results, the parameters of the 3D case (cylindrical model) are gradually reduced and it is transformed into a 2D model (disk model); and we can observe a good agreement between the results of the two simulations. Next, the simulation results are compared with the experimental results, indicating changes in lateral force. With the help of the offered dynamic model, the cantilever deformation and the forces interacting between probe tip and particle can be determined from the moment the probe tip contacts the nanoparticle to when the nanoparticle dislodges from the substrate surface.

KEYWORDS: AFM nanorobot; Nanomanipulation; Cylindrical nanoparticles; Dynamic.

1. Introduction

With the growing use of Atomic Force Microscope (AFM)-based nanorobots, the precise displacement of nanoparticles by means of these instruments has become the focus of attention. A precise manipulation process by means of an atomic microscope includes a variety of operations such as writing, touching, cutting, and displacing in nanoscale. The word "manipulation" in this paper means the exact displacement of nanoparticles. The displacement of a nanoparticle is initiated by the AFM probe tip contacting the nanoparticle as a result of the relative movement of probe and substrate. Since it is not possible to simultaneously observe the displacement of nanoparticles, there is no image of the manipulation operation while it is in progress. The only connection between the macro- and nano-worlds is the produced forces. Therefore, in order to implement the manipulation process in a controlled and accurate manner and also to automate the process, it will be necessary to simulate changes in forces during the manipulation.

In the recent decades, the researchers have focused on the use of AFMs in the transferring of nanoparticles. The first report on the displacement of spherical nanoparticles using the Scanning Tunneling Microscope (STM) was presented by Stroscio and Eigler.[1] Due to the limitations of STM and its inability in moving the non-conductive particles, there was a growth in the use of AFM for the manipulation process. Schaefer *et al.*[2] introduced the application of AFM in the displacement of nanoparticles. Subsequent research works concentrated on the displacement of various cylindrical particles on surfaces. Through the manipulation of nanotubes on various

* Corresponding author. E-mail: hkorayem@iust.ac.ir

https://doi.org/10.1017/S0263574713000854 Published online by Cambridge University Press

surfaces, Falvo *et al.*[3,4] investigated their mechanical properties as well as the different modes of motion. In recent investigations, the movement of nanowires in different modes (e.g., rotating, rolling, and sliding) has been studied experimentally.[5,6] In the conducted research works, no model for the prediction of the type of movement has been presented; and the displacement of particles has been accomplished through trial and error. So in continuation, several models are introduced for the precise performance of manipulation and the prediction of displacement of nanoparticles.

Guthold *et al.*[7] introduced a nanomanipulator instrument for displacing nanoparticles in a controlled way. For the first time, Sitti and Hashimoto[8] presented a dynamic model for the controlled manipulation of spherical nanoparticles. Then by using a dynamic model of forces and the motion modes, the researchers were able to determine the maximum force of manipulation and the moment in the dislodging of a particle from a surface.[9] Also, by using the coupled equations, the researchers have been able to dynamically solve the problem and analyze the effective parameters involved.[10] Moreover, the particle sizes that can be handled by this method have been studied.[11] With the increased use of spherical models, the researchers have tried to automate the manipulation process.[12] The models presented in the mentioned researches can be applied for the displacement of spherical particles. However, with the change of particle shape, the dynamic model also changes; and this point has been taken into consideration in the present paper. Moreover, the presented models are for the disk cases, and these do not consider the 3D conditions.

Numerous investigations have been carried out regarding the modeling of internal forces exerted on a cantilever.[13] With the growing use of V-shaped and dagger-shaped cantilevers, the use of dynamic models that apply these types of cantilevers for the manipulation and transfer of spherical nanoparticles has become widespread.[14] It should be mentioned that the introduced simulations will be used to present a 3D model that can incorporate all the possible deformations.

With the extensive use of AFM nanorobot in the displacement of cylindrical nanoparticles, the modeling of these manipulation operations has become the focus of attention. Lianqing *et al.*[15] have presented a model for the displacement of carbon nanotubes on electrodes. Other research works have concentrated on the controlled pushing of nanowires. In these investigations, the application of lateral forces has been studied to determine the conditions of motion.[16] Also, a model has been presented for the prediction of motion modes in the displacement of cylindrical particles.[17] In the most recent researches, a model that incorporates all the possible motion modes (i.e., rotating, sliding, rolling) has been presented.[18] In all the previously conducted research works, no dynamic model has been presented for the 3D modeling of forces applied on the cantilever probe tip. The 3D simulation of these forces facilitates the prediction of the manipulation process.

In this paper, first a 3D kinematic model is formulated to obtain accelerations, and then the internal forces of the cantilever are modeled. In the next step, the equations of motion are expressed on the basis of the Newton–Euler relations, and using the constant and variable parameters, the motion dynamics is simulated. Then the presented results are verified through the existing 2D simulations and by the lateral force, which has been determined experimentally. Finally, by changing the geometry and mechanical properties of the cantilever, the impact of these parameters on motion dynamics is evaluated.

2. Kinematic Modeling of the Cantilever

The use of AFM-based manipulation processes is widespread nowadays. For a controlled manipulation process, various modeling approaches have been developed. In this paper, a previous model, which simulates the 2D manipulation of sphere-shaped nanoparticles, has been improved to make the process possible for 3D cases like Carbon Nano-tubes (CNTs) or nanowires (cylindrical particles). The existing model for an AFM-based manipulation (a 2D model) has been improved in the modeling section.[9,10]

At this point, with known forces, we express the kinematics of motion for the probe tip and reference point in order to obtain the acceleration. By disregarding elastic deformations (since they are negligible) and considering the kinematic-free body diagram, the following relations are obtained in the X, Y, and Z directions. It should be pointed out that the deformations shown in the figures have

https://doi.org/10.1017/S0263574713000854 Published online by Cambridge University Press

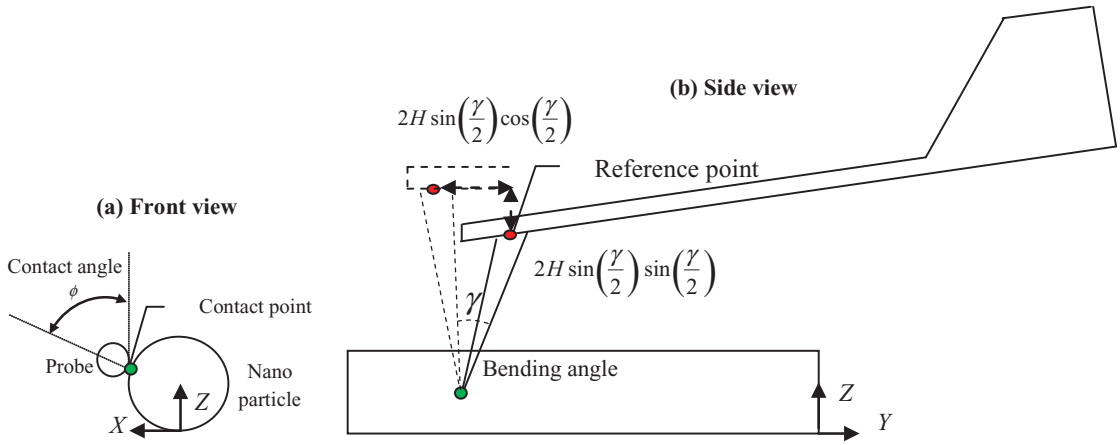


Fig. 1. (Colour online) 3D geometry of tip-particle contact: (a) Front view, (b) side view.

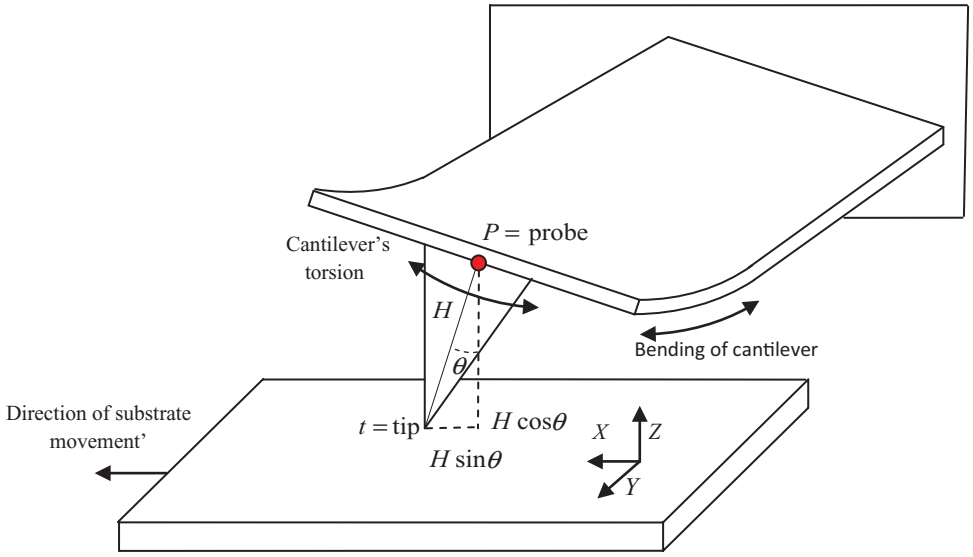


Fig. 2. (Colour online) Geometry of the connection between probe tip and reference point.

been enlarged for the sake of clarity,

$$X_p = R_p \sin\phi - H \sin\theta, \tag{1}$$

$$Z_p = R_p \cos\phi + R_p + H\cos\theta - 2H\sin^2\left(\frac{\gamma}{2}\right), \tag{2}$$

$$Y_p = 2H\sin\left(\frac{\gamma}{2}\right)\cos\left(\frac{\gamma}{2}\right). \tag{3}$$

In the above relations, the position of the reference point is defined by the X_p, Y_p, Z_p components (Fig. 1), H is the cantilever's height, R_p is the particle's radius, γ is the bending angle (an angle in the X–Y plane and caused by the force in the Y direction (Fig. 1)), θ is the twisting angle (an angle in the X–Z plane and caused by the force in the X direction (Fig. 2)), and ϕ is the contact angle (an angle in the X–Y plane, which indicates the position of the tip-particle contact point and which remains constant during the manipulation process (Fig 1)). It should be noted that the cantilever tip has been depicted as a sphere in Fig. 1.

Now, based on the presented relations, the acceleration of the reference point is determined. It should be mentioned that R_p, ϕ are the constant operation parameters, and the acceleration

https://doi.org/10.1017/S0263574713000854 Published online by Cambridge University Press

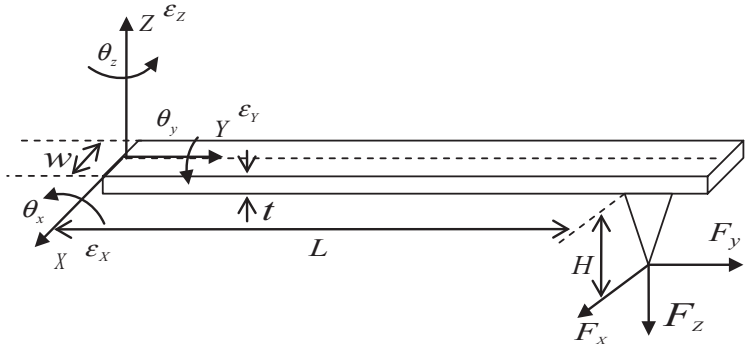


Fig. 3. Force–displacement relationship in the cantilever of AFM microscope.

components are expressed as follows:

$$\ddot{X}_p = -H\ddot{\theta}\cos\theta + H\dot{\theta}^2\sin\theta, \tag{4}$$

$$\ddot{Z}_p = -H\ddot{\theta}\sin\theta - H\dot{\theta}^2\cos\theta - 2H\ddot{\gamma}\sin\left(\frac{\gamma}{2}\right)\cos\left(\frac{\gamma}{2}\right) - H\dot{\gamma}^2\cos^2\left(\frac{\gamma}{2}\right) + H\dot{\gamma}^2\sin^2\left(\frac{\gamma}{2}\right), \tag{5}$$

$$\ddot{Y}_p = H\ddot{\gamma}\cos^2\left(\frac{\gamma}{2}\right) - H\ddot{\gamma}\sin^2\left(\frac{\gamma}{2}\right) - 2H\dot{\gamma}^2\sin\left(\frac{\gamma}{2}\right)\cos\left(\frac{\gamma}{2}\right). \tag{6}$$

In the above relations, the acceleration of the reference point is defined by the $\ddot{X}_p, \ddot{Y}_p, \ddot{Z}_p$components, $\dot{\theta}$ is the angular velocity for the twisting angle, $\ddot{\theta}$ is the angular momentum for the twisting angle, $\dot{\gamma}$ is the angular velocity for the bending angle, and $\ddot{\gamma}$ is the angular momentum for the bending angle. In the relations presented in this section, the values of $\ddot{\theta}$, $\ddot{\gamma}$ should be expressed in terms of $\dot{\theta},\ \theta,\ \dot{\gamma},\ \gamma$. Thus, in the following section, these relations have been handled considering the relative displacement of probe tip and reference point. In these relations, subscripts "p" and "t" stand for reference point and probe tip, respectively,

$$X_t = X_p + H\sin\theta, \tag{7}$$

$$Y_t = Y_p - 2H\sin\left(\frac{\gamma}{2}\right)\cos\left(\frac{\gamma}{2}\right), \tag{8}$$

$$\ddot{X}_t = \ddot{X}_p + H\ddot{\theta}\cos\theta - H\dot{\theta}^2\sin\theta, \tag{9}$$

$$\ddot{Y}_t = \ddot{Y}_p - H\ddot{\gamma}\cos^2\left(\frac{\gamma}{2}\right) + H\ddot{\gamma}\sin^2\left(\frac{\gamma}{2}\right) + 2H\dot{\gamma}^2\sin\left(\frac{\gamma}{2}\right)\cos(\frac{\gamma}{2}). \tag{10}$$

In these relations, X_t, Y_t define the tip position and $\ddot{X}_t,\ \ddot{Y}_t$ define the tip acceleration. In view of the constant speed considered for the substrate, it can be assumed that the expressed relative accelerations are equal to zero; therefore, the values of $\ddot{\theta}$, $\ddot{\gamma}$ are defined in terms of $\dot{\theta},\ \theta,\ \dot{\gamma},\ \gamma$,

$$\ddot{\theta} = \dot{\theta}^2\tan\theta, \tag{11}$$

$$\ddot{\gamma} = 2\dot{\gamma}^2\frac{\sin\left(\frac{\gamma}{2}\right)\cos\left(\frac{\gamma}{2}\right)}{\cos^2\left(\frac{\gamma}{2}\right) - \sin^2\left(\frac{\gamma}{2}\right)}. \tag{12}$$

3. Modeling of Forces Exerted on the Cantilever

The internal forces should be determined to obtain the dynamic model of motion. In this section, by combining the existing models,[9,10,13] a 3D model will be presented, which depicts the relationship between internal forces and deformations. In this analysis, as shown in Fig. 3, three forces are applied on the probe tip in the X, Y, and Z directions, which cause six deformations in the ε_X, ε_Y, and ε_Z directions as well as three rotations of θ_X,θ_Y,and θ_Z.

https://doi.org/10.1017/S0263574713000854 Published online by Cambridge University Press

First, the application of force in the Z direction (F_Z) has been considered. Due to the application of F_Z, the cantilever bends along the Z direction, and the end of cantilever displaces downward along the Z direction,[9,13]

$$K_Z = \frac{Ewt^3}{4L^3}. \tag{13}$$

In Eq. (13), E is the modulus of elasticity, w is the cantilever's width, t is the cantilever's thickness, and L is the cantilever's length. Next, the effect of force in the X direction (F_X) is examined. This force causes two deformations in the cantilever: the displacement of the probe tip along the x-axis, and the twisting of the probe about the y-axis. The relations corresponding to these deformations are presented below. Similar to the previous case, the effect of F_X is modeled as bending by using the constant K_X,[9,13]

$$K_X = \frac{Etw^3}{4L^3}. \tag{14}$$

Contrary to force F_Z, the moving of which was possible along its own line of action without producing a moment, force F_X produces a torque with magnitude $T = F_X \times H$, where H is the height of the probe tip. By substituting $G = \frac{E}{2(1+\upsilon)}$($\upsilon$ is the Poisson's ratio and G is the shear modulus) into the relation, this deformation can be modeled by using the constant K_{θ_Y},[9,13]

$$K_{\theta_Y} = \frac{1}{6} \times \frac{Ewt^3}{L(1+\upsilon)}. \tag{15}$$

Finally, we investigate the effects of the force applied in the Y direction (F_Y). This force affects the cantilever in two ways. It produces bending along the X direction as well as displacement in the Z direction. The relations associated with these deformations and the relevant spring constants are presented below,[9,13]

$$K_{\theta_X} = \frac{Ewt^3}{12L}. \tag{16}$$

By moving force F_Y, we observe a displacement along the Y direction, whose relevant spring constant is obtained from the following relation,[9,13]

$$K_Y = \frac{Ewt}{L}. \tag{17}$$

Considering the relations obtained in the previous steps, the 3D cantilever deformation can be obtained through the following relations by using the spring constants. These relations enable us to observe the 3D displacement of the cantilever. In the following relations, H is the cantilever height. By substituting the above relations into the deformation matrix, changes of internal forces can be determined based on spring constants and deformations:

$$\begin{bmatrix} F_X \\ F_Y \\ F_Z \end{bmatrix} = \begin{bmatrix} K_X & 0 & 0 & 0 & \frac{K_{\theta_Y}}{H} \\ 0 & K_Y & 0 & \frac{K_{\theta_X}}{H} & 0 \\ 0 & 0 & K_Z & 0 & 0 \end{bmatrix} \times \begin{bmatrix} \varepsilon_X \\ \varepsilon_Y \\ \varepsilon_Z \\ \theta_X \\ \theta_Y \end{bmatrix}. \tag{18}$$

In the above relation, $F_X,\ F_Y,\ F_Z$ are the applied forces, $K_X,\ K_Y,\ K_Z,\ K_{\theta_X},\ K_{\theta_Y}$ are the spring constants, $\varepsilon_X,\ \varepsilon_Y,\ \varepsilon_Z$ are the displacements, and $\theta_X,\ \theta_Y$ are the angular displacements. It should be pointed out that due to the lack of cantilever deformation in the Y direction, deformation along this direction can be assumed as constant, and the forces applied on cantilever can be modeled using four springs ($K_X,\ K_Z,\ K_{\theta_Y},\ K_{\theta_X}$).

https://doi.org/10.1017/S0263574713000854 Published online by Cambridge University Press

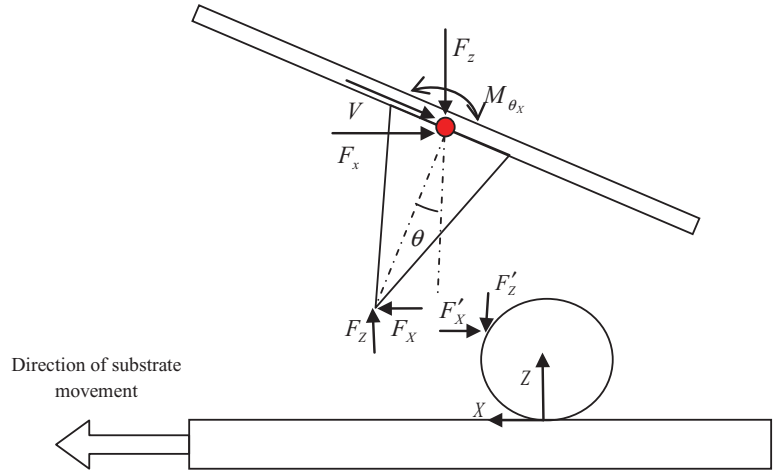


Fig. 4. (Colour online) Diagram of forces applied on the cantilever (front view).

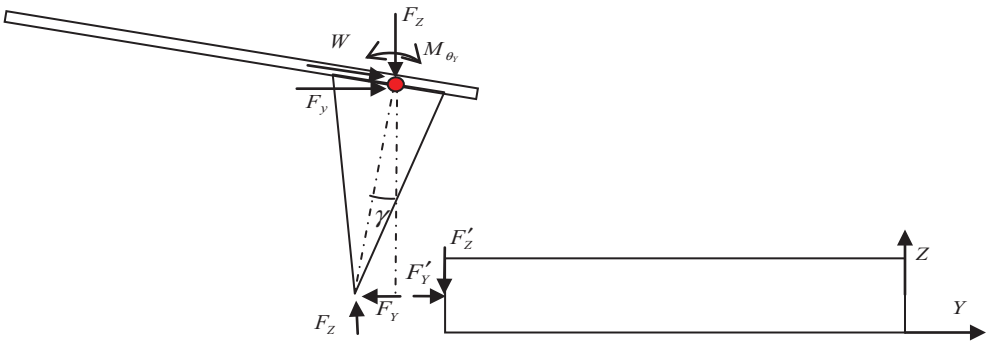


Fig. 5. (Colour online) Diagram of forces applied on the cantilever (side view).

4. Modeling the Governing Manipulation Dynamics of Cylindrical Nanoparticles

In this section, the existing model of an AFM-based manipulation has been improved.[9,10] In order to investigate and present a dynamic model, first, it would be necessary to have a free body diagram which displays the forces involved and how they are applied. In the front and side views shown in Figs. 4 and 5, all the possible forces that could be applied on the probe tip, along with their reactions, have been illustrated. F_X, F_Y, F_Z represent the external forces applied on the probe tip by the surrounding environment. These forces cause a 3D displacement of the probe tip and produce internal forces and moments of F_x, F_y, F_z, $M_{\theta X}$, $M_{\theta Y}$, W, V, which have been shown in the following figures. An approach similar to the one employed in the dynamic modeling of the 2D case is used in this modeling procedure.[9]

After presenting the free body diagrams of the cantilever and applied forces, the Newton–Euler equations and the relevant free body diagrams are used to obtain dynamic equations. At this point, we will arrange and organize F_X, F_Y, F_Z, W, V in terms of other forces and displacements and obtain the dynamic relations of forces. Taffazzoli[9] has used a similar approach in obtaining the dynamics of spherical nanoparticles in the 2D case. It should be noted that the required accelerations are determined regarding 3D kinematics,

$$\begin{aligned} F_Z &= \left(\frac{I\ddot{\theta} + M_{\theta_X}}{H}\right)\sin\theta - ma_x \sin\theta\cos\theta - F_x \sin\theta\cos\theta \\ &\quad + F_z\cos^2\theta + ma_z\cos^2\theta + W\sin\gamma\cos^2\theta, \\ F_Y &= \left(\frac{I\ddot{\gamma} + M_{\theta_Y}}{H}\right)\cos\gamma - F_z\sin\gamma\cos\gamma - V\sin\theta\cos\gamma\sin\gamma \end{aligned} \tag{19}$$

https://doi.org/10.1017/S0263574713000854 Published online by Cambridge University Press

Table I. Geometrical specifications and mechanical properties of cantilever.

Process constants		Mechanical properties			Geometrical specifications			
Probe tip distance along Z direction, Z_t	Contact angle, ϕ	ρ $\left(\frac{\text{kg}}{\text{m}^3}\right)$	ν	E (Gpa)	Probe height, H	Cantilever thickness, t	Cantilever width, w	Cantilever length, L
$Z_L = H + L\sin(0.7)$ $Z_L = 1.47 \times 10^{-5}$	45°	2330	0.27 μm	169	12 μm	1 μm	48 μm	220 μm

$$-ma_z \cos\gamma \sin\gamma - ma_y \sin^2\gamma + F_y \sin^2\gamma, \tag{20}$$

$$V = \frac{1}{\sin\theta}(F_Z - F_z - w\sin\gamma - ma_z), \tag{21}$$

$$w = \frac{1}{\sin\gamma}(F_Z - F_z - v\sin\theta - ma_z), \tag{22}$$

$$F_X = ma_x + F_x + V\cos\theta, \tag{23}$$

$$F_T^2 = F_X^2 + F_Y^2 + F_Z^2, \tag{24}$$

In the above relations, F_x, F_y, F_z, M_{θ_X}, M_{θ_Y}, W, V are the components of internal forces and momentums, F_X, F_Y, F_Z are the components of dynamic forces, F_T is the norm of dynamic forces, a_x, a_y, a_z are the components of probe's acceleration, and m and I are the tip's mass and moment of inertia, respectively.

5. Dynamic Simulation of Cylindrical Nanoparticles Manipulation

In order to simplify the simulation of the dynamic motion, the velocity of the substrate as well as the contact angle between probe tip and particle are assumed as constant. A constant contact angle means that the probe tip is fixed and will not move on the particle's surface. At this point, the geometrical and mechanical constants and the process constants (including the particle–probe contact angle and the constant value of Z_t (height of probe tip)) are included in the simulation process using Table I. Also, the simulation time, during which the dynamic forces change, is specified. It should be noted that at $t = 0$, θ is equal to 0; so $\sin(\theta)$ in Eq. (19) through (22) goes to zero and causes a singularity. This condition has occurred in previous works as well,[9,10,12,18] so the conditions of motion are set for $t = 0.2$ s.

There are five phases in the presented simulation (Fig. 8). In the first phase the constant values are obtained. In the second phase, the process variables, which change during each time interval, are determined. To obtain θ, which is one of the main parameters of motion, two methods have been proposed.[9,10] In the first method, a set of second-order ordinary differential equations (ODEs) has been solved using the Runge–Kutta numerical solution[9,12] and thus dynamic parameters $(X_p, \dot{X}_p, \theta, \dot{\theta})$ have been obtained. In the second approach, the dynamic parameters have been introduced by taking into consideration the substrate speed and geometrical relations.[10] In both methods, the dynamic parameters have been obtained in a time frame. In this paper, deformations $(X_p, \dot{X}_p, \theta, \dot{\theta})$ have been introduced using the previous work.[9] Also, the values of γ, $\dot{\gamma}$, Y_p, $\dot{Y}_p$ have been considered as 20% of the above deformations. Using Figs. 6 and 7, eight variable parameters are introduced into the simulation algorithm. Now by knowing the variable parameters and using the coupled equations method,[10] the dynamic forces could be defined. These equations are expressed for each time-step by using the constant and dynamic parameters.

In the third phase of the simulation, the simulation is performed by obtaining the constant parameters and using the described dynamic parameters, which can be defined for any desired time-step and time interval (we used 0.23 s for the time interval and 0.01 for the time-step). As explained, we use the dynamic and constant parameters at t = 0.02 s (initial time). In this step, the accelerations of motion of the reference point are known, and the internal forces can be included in the simulation process as well. Thus, all the required parameters for determining the forces in this time interval are obtained.

https://doi.org/10.1017/S0263574713000854 Published online by Cambridge University Press

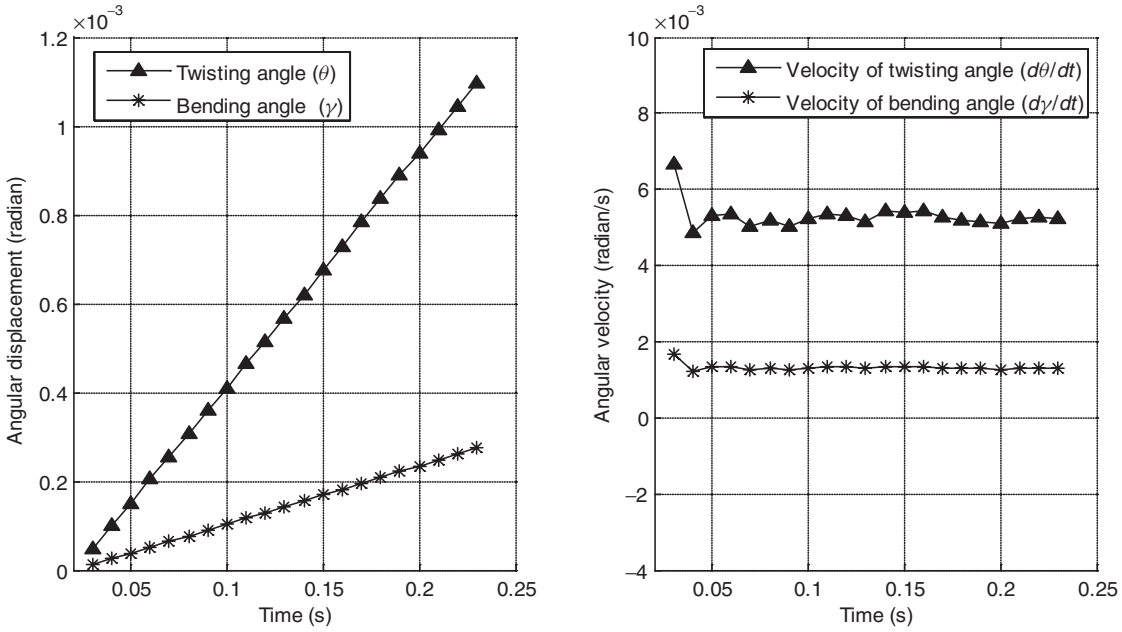


Fig. 6. Displacements of $\theta, \dot{\theta}, \gamma, \dot{\gamma}$ (variable parameters) achieved through the simulations of the disk case and its generalization.

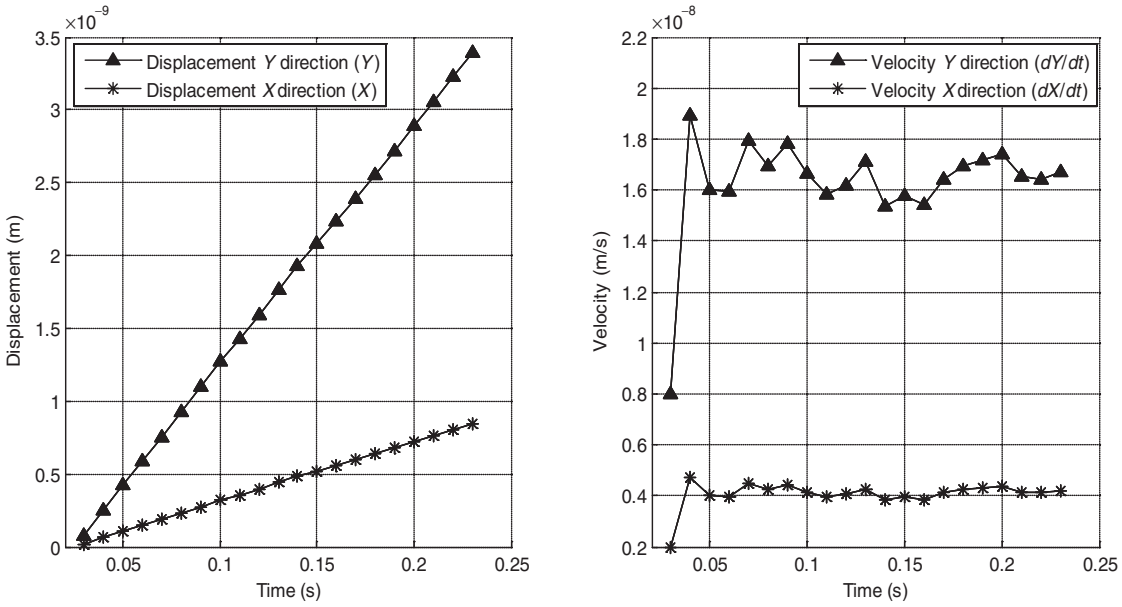


Fig. 7. Displacements of $X_p,\ \dot{X}_p,\ Y_p,\ \dot{Y}_p$ (variable parameters) achieved through the simulations of the disk case and its generalization.

In the fourth phase of the simulation, all the specified parameters are incorporated into the coupled equations.[10] By using these coupled equations, the dynamic forces ($F_Z,\ F_X,\ F_Y$) are determined and the simulation process is completed.

In the final phase of the simulation, the presumed simulation time (the initial time, t = 0.02 s) is compared with the time interval established in the second phase (considered as 0.23 s in this simulation). If the time interval is different from the initial time, 0.01 s (time-step) will be added to the initial time; consequently a new initial time of t = 0.03 s will be obtained and phases three through five will be repeated. This procedure will continue until the two mentioned times become equal. Ultimately, the force–time diagram is obtained for the specified time interval.

https://doi.org/10.1017/S0263574713000854 Published online by Cambridge University Press

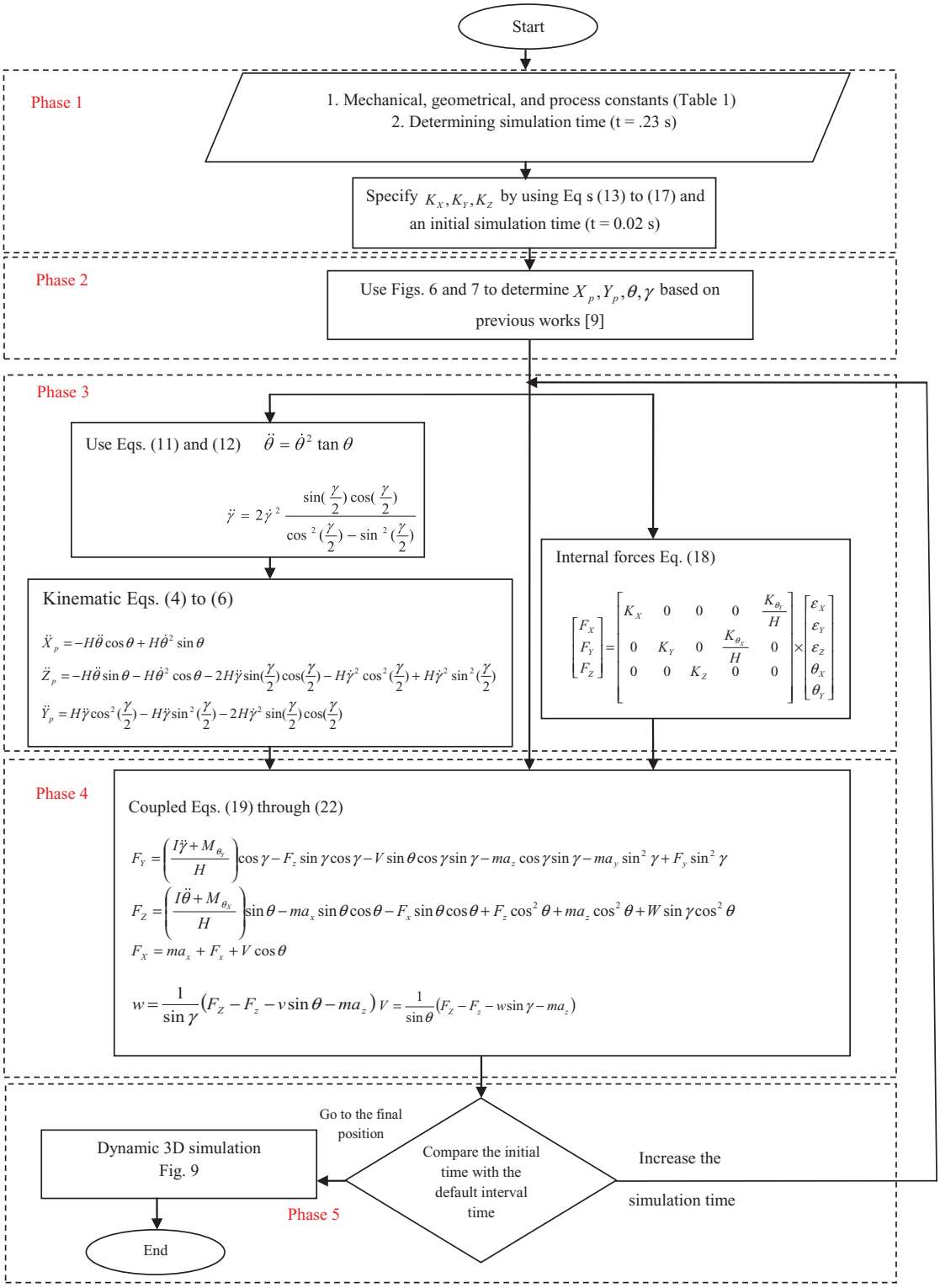


Fig. 8. (Colour online) Simulation algorithm for the manipulation of cylindrical nanoparticles.

As is shown, and expected, the most effective force is applied in the perpendicular Z direction (Fig. 9). In the results presented by Tafazzoli,[9] a similar situation has been observed in the manipulation of spherical particles. This is caused by severe deformation of cantilever along the Z direction, which produces a force of large magnitude at the initial moment of impact. As time passes, no new displacement occurs in the Z direction, and the forcein this direction remains constant throughout

https://doi.org/10.1017/S0263574713000854 Published online by Cambridge University Press

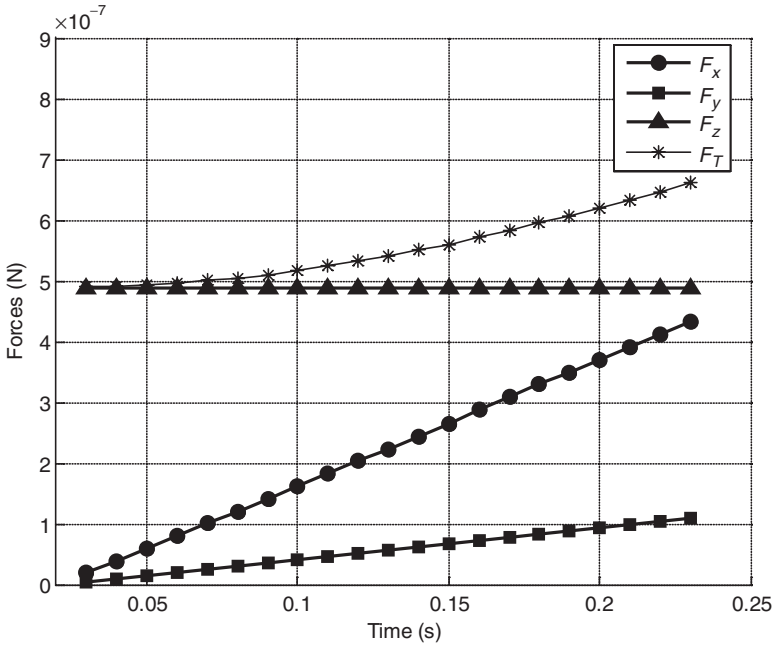


Fig. 9. Simulation of forces F_X, F_Y, F_Z and the resultant force F_T.

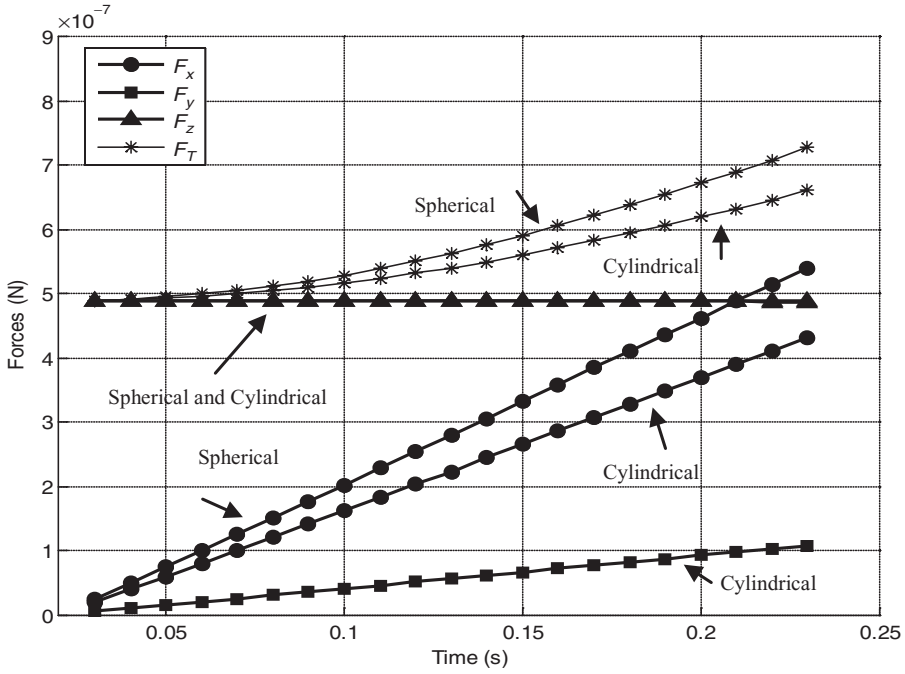


Fig. 10. Simulation of forces F_X, F_Y, F_Z and the resultant force F_T in 2D (simulation of spherical particles) and 3D (simulation of cylindrical particles) cases.

the operation. However, in the X direction, along which the lateral force is modeled, an increasing force is produced, which pushes the particle and causes it to move. This main force of manipulation increases up to the threshold magnitude needed for particle movement; and after the movement of the particle, the mentioned force remains constant. Another force is produced along the Y direction due to the bending of probe about the X-axis, and it increases along with F_X. Of course, the magnitude of this force is much less than that of F_X. The resultant force (F_T), which is applied to the AFM's probe tip and represents the resultant of all three forces based on Eq. (24), has been investigated in

https://doi.org/10.1017/S0263574713000854 Published online by Cambridge University Press

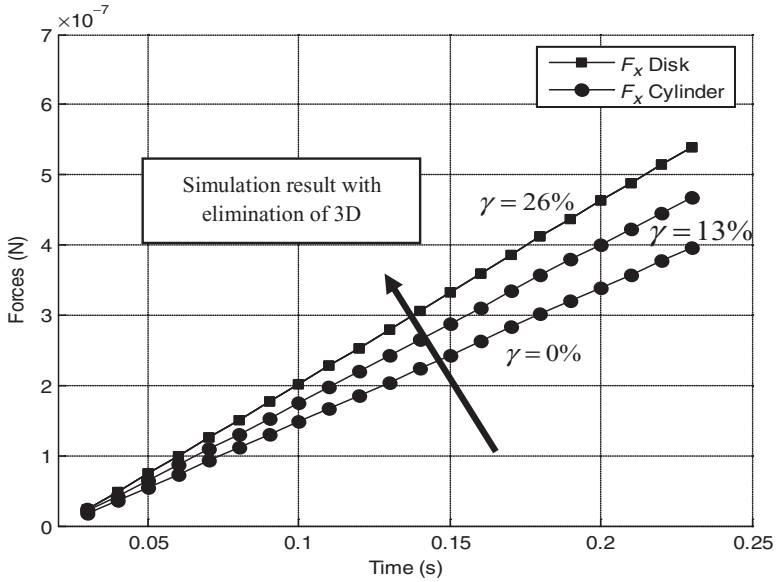


Fig. 11. Results of 3D simulation of the force along the *X* direction when it approaches the 2D format.

the following section. As expected, this force starts with a constant magnitude at the initial moments of the movement and increases afterwards.

If the simulations of 3D and 2D cases, which are respectively used in the manipulations of cylindrical and spherical particles, are presented together in one diagram, it will be observed that force F_Y (which exists in the 3D case), is not present in the 2D case. Also, as expected, the main manipulation force in the 3D case has become less than that in the 2D case. This facilitates the prediction of movement regarding experimental results. The difference between F_Y forces in the two cases is so small that, as Fig. 10 illustrates, these two forces completely match each other in the shown interval; and to be able to differentiate between these two forces, the interval in which they change should be made smaller. The difference between these two cases has been discussed in the following section.

6. Validation of Dynamic Simulation of Cylindrical Nanoparticles Manipulation

In order to validate the presented dynamic simulations, the simulations of the spherical case are used. In the existing research works, the manipulation dynamics represent disk cases (2D formats); so for the sake of comparison, by eliminating the 3D parameters of the presented simulations, we transform them from 3D to 2D cases.

Next, changes in forces in different directions have been reviewed. As stated previously, in the presented dynamic models, the manipulation of cylindrical nanoparticles has been modeled in a 3D format. The two forces of F_X, F_Z are common in the presented 3D and disk models. First, we study the change of F_X. At this point, by reducing the effects of 3D parameters in the cylindrical model, we bring the results closer to those of the 2D model. It is observed in Fig. 11 that the results of the 3D model approach those of the 2D model.

Similarly, in the simulation of force F_Z, when the effects of 3D simulation parameters are reduced, both models display a similar behavior; and with the complete elimination of these effects, both simulations match each other. It should be pointed out that the range of changes in F_Z is very small (Fig. 12).

Now we examine changes in force F_Y, which appears in the 3D simulation. As stated previously, this force emerges in the 3D configuration; therefore, when the effective parameters in the 3D model approach zero, the simulated values of F_Y also approach zero; and when the parameters of the 3D model become zero, the magnitude of force F_Y also becomes zero (Fig. 13).

Considering the stated information and the presented simulations, it is observed that by gradually eliminating the effective parameters in the 3D model through a specific mechanism, the answers

https://doi.org/10.1017/S0263574713000854 Published online by Cambridge University Press

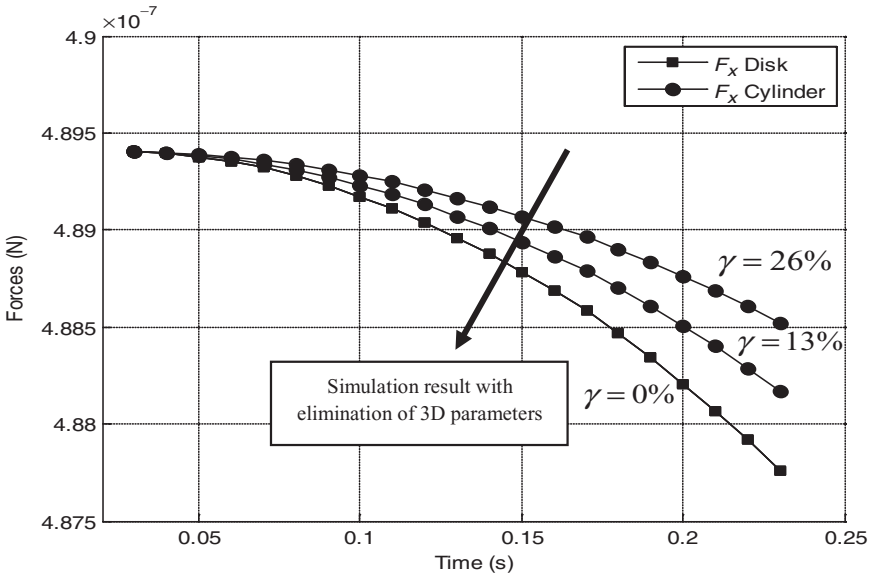


Fig. 12. Results of 3D simulation of the force along the *Z* direction when it approaches the 2D format.

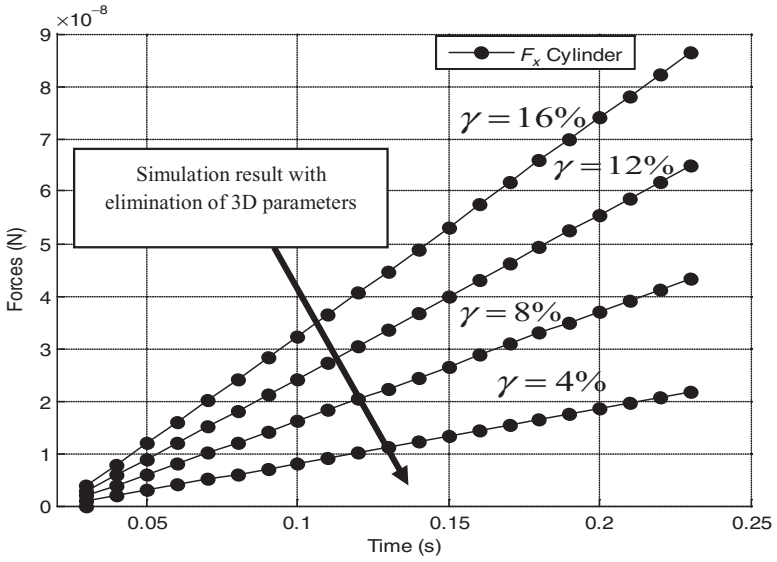


Fig. 13. Results of 3D simulation of the force along the *Y* direction when it approaches the 2D format.

approach those of the 2D configuration. So by applying the presented algorithm, we would be able to precisely simulate the motion behavior of nanoparticles in 3D format.

In continuation, experimental tests are used to validate the presented simulations, and the obtained results have been evaluated. Since a direct observation of the nanomanipulation process is not possible, the movement in the nano-environment is investigated through the applied forces. Of the forces exerted along the *X*, *Y*, and *Z* directions, F_X (which is applied laterally on the cantilever) is highly important. This force can be investigated by the atomic force microscope via the Lateral Force Microscopy (LFM) mode. The performed experiments in Hsu and Chang[16] show changes in the lateral force during the process. In these experiments, a carbon nanotube with the diameter of 100 nm and length of 4.2 μm and another nanotube with the diameter of 60 nm and length of 1.8 μm have been pushed. In the paper presented by Hsu and Chang,[16] the speed of the substrate has been considered as 0.1 μm/s, and the presented diagram has been plotted based on the location of the probe tip and the lateral force. By knowing the speed of the substrate and the location of the probe tip, the force–time diagram can be obtained.

https://doi.org/10.1017/S0263574713000854 Published online by Cambridge University Press

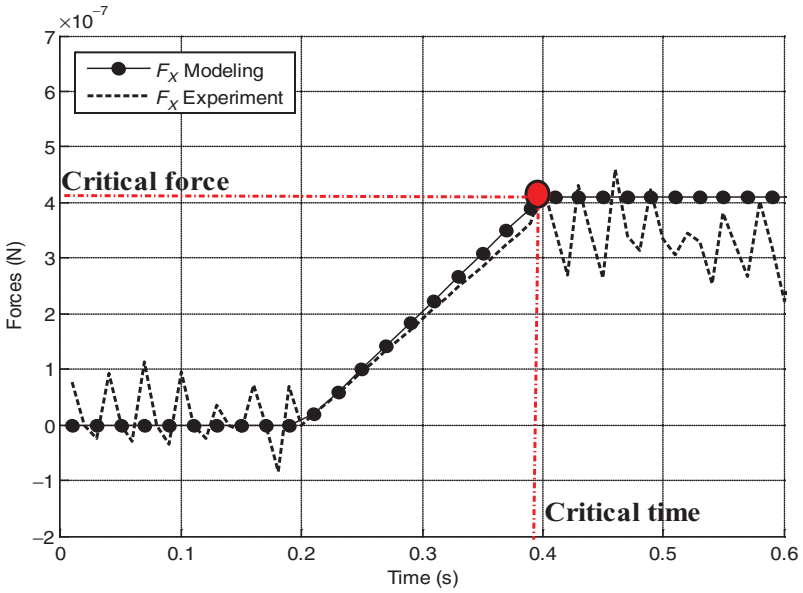


Fig. 14. (Colour online) Simulation of lateral force on a cylindrical nanoparticle (diameter = 60 nm, length = 1.8 μm) in a laboratory setting[16] and in the presented modeling.

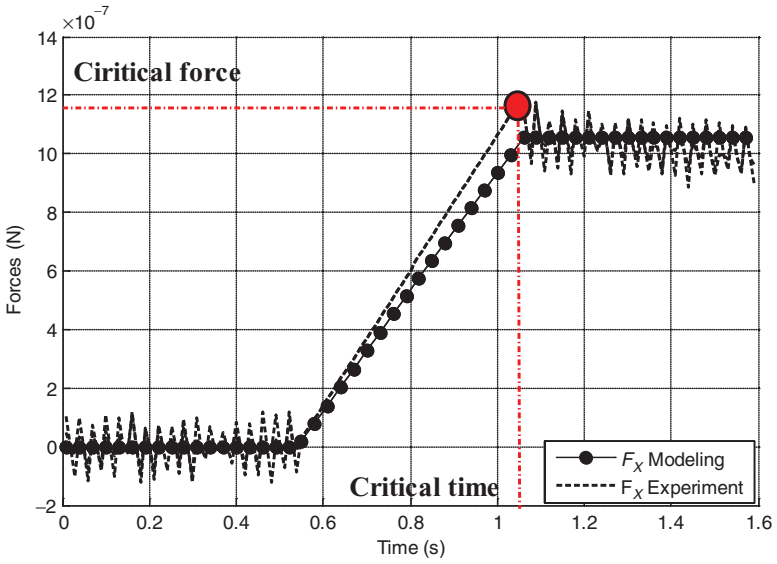


Fig. 15. (Colour online) Simulation of lateral force on a cylindrical nanoparticle (diameter = 100 nm, length = 4.2 μm) in a laboratory setting[16] and in the presented modeling.

In these lateral force diagrams, first, there is a contact between the probe tip and the substrate. This contact is continually maintained on the surface and leads to the creation of a constant force, which is disregarded in the investigation. As illustrated in Fig. 14, at the moment of impact, the lateral force, which is the main pushing force in the X direction, shows an increase in magnitude. This process continues until the nanoparticle starts to move. At this point, the pushing force reaches its peak value in the diagram (Fig 14). The critical time (the time at which the particle starts to move on the substrate) and the critical force (maximum manipulation force that appears during the process) have been presented in Figs. 14 and 15, respectively. The maximum pushing force for the cylindrical nanoparticle with the diameter of 100 nm and length of 4.2 μm is 1250 nN, and it occurs at t = 0.5 s; and for the nanotube with the diameter of 60 nm and length of 1.8 μm, the maximum pushing force is 350 nN, which occurs at t = 0.2 s.

https://doi.org/10.1017/S0263574713000854 Published online by Cambridge University Press

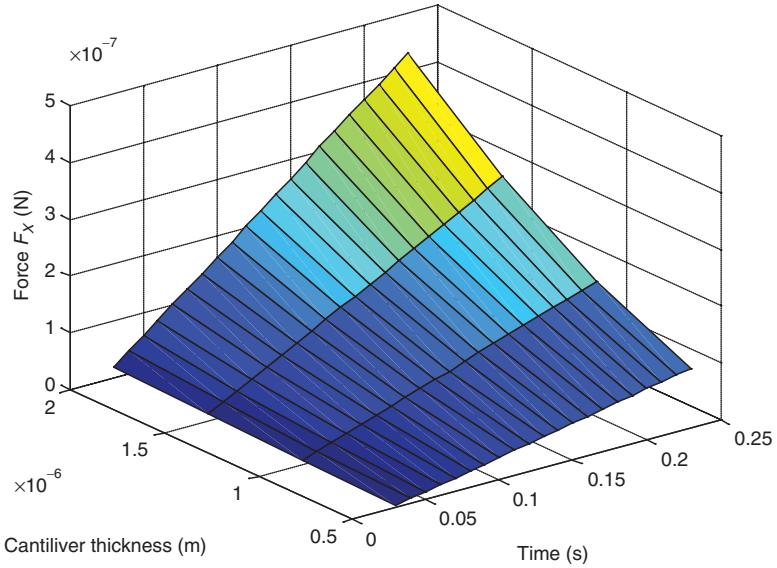


Fig. 16. (Colour online) Simulation of changes in force F_X with cantilever thickness t.

Now by using the information obtained from the experimental results, the force–time diagrams and the simulation results of the proposed model are presented together in a diagram for the purpose of comparison and evaluation. As observed, under similar conditions, the simulation results have adequate agreement with the experimental results; and thus the presented model is validated.

7. Simulation of Effective Parameters in the Dynamic Manipulation of Cylindrical Particles

In previous works, the effective parameters have been investigated to find the effect of geometrical process and environmental parameters.[9,10,12,13,17,18] The defined dynamic model is deeply dependent on geometrical parameters. In general, the stiffer cantilevers develop higher forces. However, as a result of an extensive range of geometrical parameters (e.g., cantilever length varies from 150 to 350 μm, and cantilever thickness (t) varies from 0.5 to 2 μm), it is not clear which parameter is most effective. Moreover, although the height of a cantilever does not have a direct impact on its stiffness, it influences the presented dynamic model, so it should be investigated. To demonstrate the changes in the presented model against the changes in effective parameters, the impact of each of these parameters is determined in the presented simulations.

Consequently, there are two main goals in this section. First, finding the most effective parameter that causes the highest change, in general, and second, finding the most drastic change within the defined intervals.

First, cantilever thickness (t) is made to vary from 0.5 to 2.0 μm, and the impact of this change is investigated. Forces F_X, F_Y, F_Z change as the cantilever thickness (t) varies in the said range. As indicated by the presented simulations, with increase in cantilever thickness from 0.5 to 2.0 μm, the magnitude of all the three forces and that of the resultant force increases. The increase of forces in this case is more drastic, relative to other simulation cases, and it is observed that for a small change in cantilever thickness, there is a severe change in the magnitude of force in all the three directions (Fig. 16).

Another geometric parameter that has been considered is cantilever length, L, which is changed from 150 to 300 μm. With increase in cantilever length, the mechanical strength of the cantilever, and consequently its resistance against force, diminishes. Hence, we witness a reduction of forces in Fig. 17, and the magnitude of all the three forces of F_X, F_Y, F_Z diminishes as a result.

In this section, the parameter of probe tip height, H, has been investigated. The height of probe tip has been increased from 12 to 18 μm, and the results of these changes have been shown in the performed simulations. By increasing the height of probe tip, the location and distance of the point at which the force is applied increases and consequently the probe's mechanical strength diminishes

https://doi.org/10.1017/S0263574713000854 Published online by Cambridge University Press

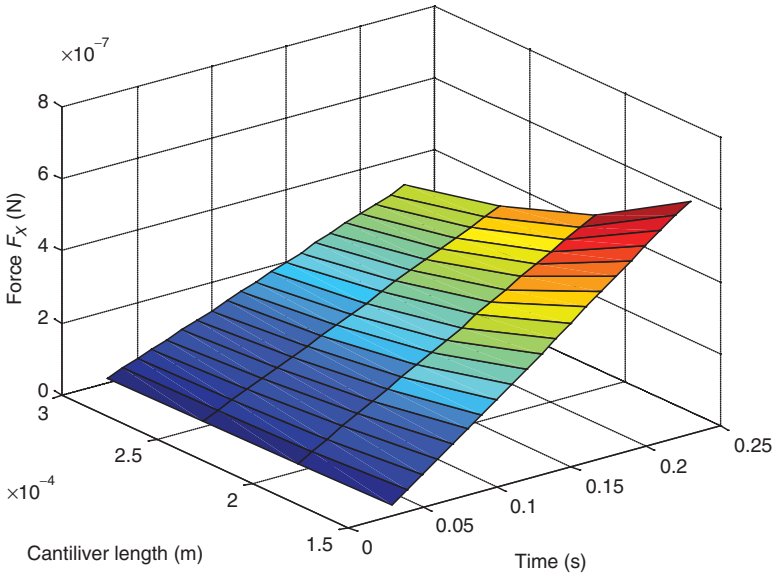


Fig. 17. (Colour online) Simulation of changes in force F_X with cantilever length L.

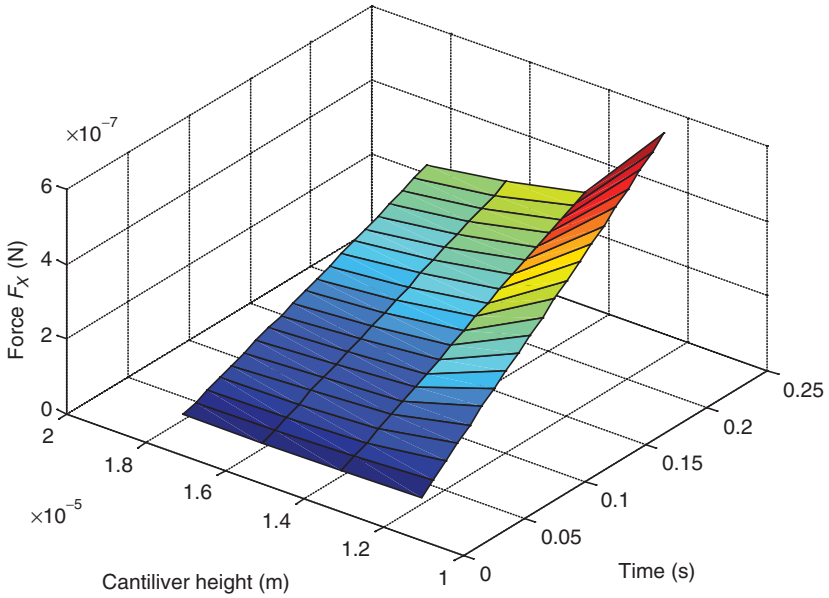


Fig. 18. (Colour online) Simulation of changes in force F_X with cantilever's probe tip height H.

and the applied forces are reduced. As observed in Fig. 18, with increase in probe tip height, all the three forces of F_X, F_Y, F_Z diminish in magnitude.

Next, the impact of cantilever width, w, has been examined. Cantilever width has been increased from 35 to 50 μm, and the obtained simulation results have been evaluated. With increase in cantilever width, the strength and stiffness of cantilever also increase, and as a result the applied forces increase in magnitude (see Fig. 19).

Finally, the effect of elasticity modulus, E, has been investigated. Modulus of elasticity has been increased from 150 to 225 Gpa. It is observed that because of this increase, cantilever stiffness has gone up, and consequently the dynamic forces have increased in all the three directions (see Fig. 20).

Considering the above-mentioned findings, it is observed that factors such as cantilever's elasticity modulus, width, and thickness, whose increase adds to the strength and rigidity of the cantilever, also cause the applied forces to increase, and that with reduction of these factors, there is decrease in applied forces. Three-dimensional presentations help us to demonstrate both the magnitude and

https://doi.org/10.1017/S0263574713000854 Published online by Cambridge University Press

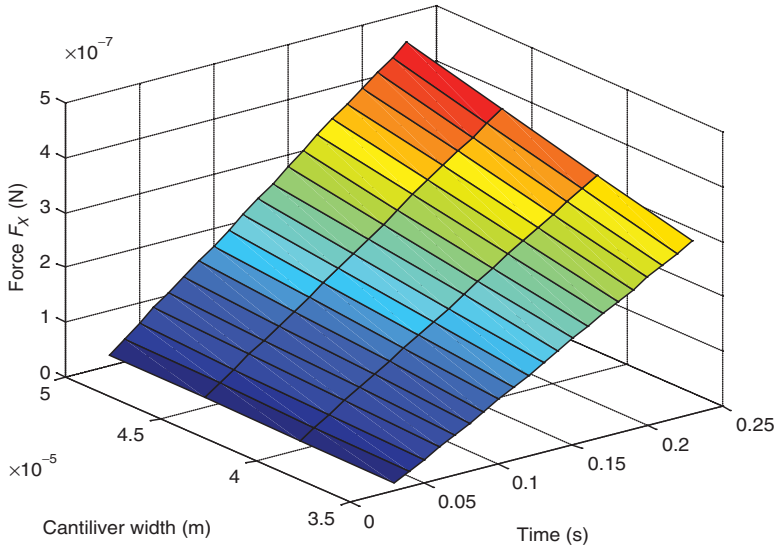


Fig. 19. (Colour online) Simulation of changes in force F_X with cantilever width w.

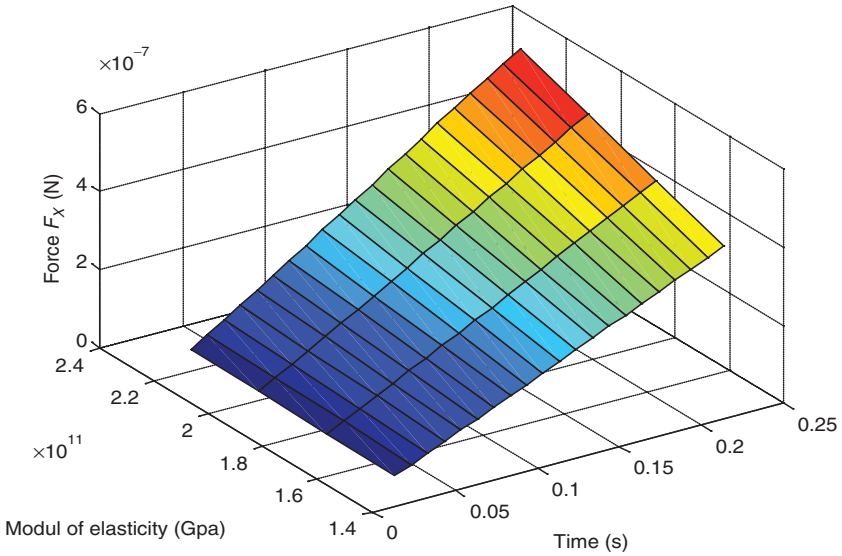


Fig. 20. (Colour online) Simulation of changes in force F_X with cantilever's modulus of elasticity E.

variation of forces within the defined ranges. Within these ranges, the shortest cantilever develops the highest force. However, the presented simulations indicate that the most influential parameter is the cantilever thickness.

8. Conclusions

Considering the fact that the forces involved in the moving and displacing of cylindrical nanoparticles need to be investigated in all the three directions, this paper has presented a model by which changes in these forces in 3D condition can be predicted. Using the presented simulation and the Virtual Reality environment, all the effective forces in the displacement of cylindrical nanoparticles can be predicted by means of an AFM nanorobot. Since the forces are the only means of connection between the nano- and macro-worlds, the ability to know and understand these forces is very important.

In this paper, all three forces of F_X, F_Y, F_Z have been simulated. The most widespread change of force is associated with the lateral force F_X, which is in fact the major force of the operation. This force changes from 0.18 to 4.3 μN. In the presented simulations, the least amount of change

https://doi.org/10.1017/S0263574713000854 Published online by Cambridge University Press

is associated with the vertical force F_Z. As the operation mechanism shows, first, a small vertical displacement is produced, which due to high sensitivity toward cantilever, appears as a vertical force F_Z with a magnitude of 4.8 μN. However, since the induced deformation does not change with time, this force remains almost constant. Force F_Y is a lateral force similar to F_X, but with smaller changes, and it varies in the range of 0.04–0.1 μm.

Also, all the influential parameters in the presented nonlinear dynamic modeling have been examined in this paper. The change in the cantilever thickness has caused the most drastic changes in the involved forces. By changing the cantilever thickness from 1.0 to 2.0 μm, the main force of manipulation (F_X) becomes 48 μN; therefore, in implementing the manipulation process, substantial attention should be paid to this parameter. It should be noted that within the specified ranges, cantilever with a length of 150 μm develops the highest magnitude force.

By completing the simulations presented in this paper and using the motion modes, the critical time and force can be predicted. Therefore, these simulations are able to improve and facilitate the precise displacement of cylindrical nanoparticles. The first step in predicting the movement of cylindrical particles is to determine the dynamic forces involved in the manipulation process, which has been presented in this paper.

References

1. J. A. Stroscio and D. M. Eigler, "Atomic and molecular manipulation with the scanning tunneling microscope," *Science* **254**(5036), 1319–1326 (1991).
2. D. M. Schaefer, R. Reifenberger, A. Patil and R. P. Andres, "Fabrication of two-dimensional arrays of nanometer-size clusters with the atomic force microscope," *Appl. Phys. Lett.* **66**(8), 1012–1014 (1995).
3. M. R. Falvo, G. Clary, A. Helser, S. Paulson, R. M. Taylor II, V. Chi, F. P. Brooks, Jr., S. Washburn and R. Superfine, "Nanomanipulation experiments exploring frictional and mechanical properties of carbon nanotubes," *Microsc. Microanal.* **4**(5), 504–512 (1999).
4. M. R. Falvo, J. Steele, R. M. Taylor II and R. Superfine, "Gear like rolling motion mediated by commensurate contact: Carbon nanotubes on HOPG," *Phys. Rev.* B, **62**(16), 10665–10667 (2000).
5. E. Gnecco, A. Rao, K. Mougin, G. Chandrasekar and E. Meyer, "Controlled manipulation of rigid nanorods by atomic force microscopy," *Nanotechnology* **21**(21), 1–5 (2010).
6. E. Tranvouez, A. Orieux, E. Boer-Duchemin, C. H. Devillers, V. Huc, G. Comtet and G. Dujardin, "Manipulation of cadmium selenide nanorods with an atomic force microscope," *Nanotechnology* **20**(16), 1–10 (2009).
7. M. Guthold, M. R. Falvo, W. G. Matthews, S. Paulson, S. Washburn, D. Erie, R. Superfine, F. P. Brooks and R. M. Taylor, "Controlled manipulation of molecular samples with the nanomanipulator," *IEEE-ASME Trans. Mechatronics* **5**(2), 189–198 (2000).
8. M. Sitti and H. Hashimoto, "Controlled pushing of nanoparticles: Modeling and experiments," *IEEE-ASME Trans. Mechatronics* **5**(2), 199–211 (2000).
9. A. Tafazzoli, "Atomic Force Microscope Based Two-Dimensional Micro/Nano Particle Manipulation and Assembly," *Ph.D. thesis*, Carnegie Mellon University (CMU), Pennsylvania, United States (2005) pp. 23–61.
10. M. H. Korayem and M. Zakeri, "Sensitivity analysis of nanoparticles pushing critical conditions in 2D controlled nanomanipulation based on AFM," *Int. J. Adv. Manuf. Technol.* **41**(7–8), 714–726 (2009).
11. C. D. Onal, O. Ozcan and M. Sitti, "Automated 2D nanoparticle manipulation using atomic force microscopy," *IEEE Trans. Nanotechnol.* **10**(3), 472–481 (2011).
12. M. H. Korayem, A. K. Hoshiar and N. Ebrahimi, "Maximum allowable load of atomic force microscope (AFM) nanorobot," *Int. J. Adv. Manuf. Technol.* **43**(7–8), 690–700 (2009).
13. K. Daeinabi and M. H. Korayem, "Nano-Manipulator Force Transducer Modeling Based on Atomic Force Microscopy," **In**: *Proceedings of the 9th IEEE Conference on Nanotechnology*, Genoa (2009) pp. 896–899.
14. K. Daeinabi, M. H. Korayem and S. A. Yarijani, "Spring constant analysis of the AFM rectangular, v-shaped and dagger cantilever probes," *Micro Nano Lett.* **6**(12), 1007–1011 (2011).
15. L. Lianqing, Y. Peng, T. Xiaojun, W. Yuechao, D. Zaili and X. Ning, "Force Analysis of Top-Down Forming CNT Electrical Connection Using Nanomanipulation Robot," **In:** *Proceedings of the International Conference on Mechatronics and Automation*, Luoyang, Henan (2006) pp. 113–117.
16. J. H. Hsu and S. H. Chang, "Tribological Interaction Between Multi-Walled Carbon Nanotubes and Silica Surface Using Lateral Force Microscopy," *Wear* **266**(9–10), 952–959 (2009).
17. M. Moradi, A. H. Fereidon and S. Sadeghzadeh, "Aspect ratio and dimension effects on nanorod manipulation by atomic force microscope," *Micro Nano Lett.* **5**(5), 324–327 (2010).
18. M. H. Korayem and A. K. Hoshiar, "Modeling and simulation of dynamic modes in the manipulation of nanorods," *Micro Nano Lett.* **8**(6), 284–287 (2013).

https://doi.org/10.1017/S0263574713000854 Published online by Cambridge University Press